Self-Assembly of a Metal–Phenolic Sorbent for Broad-Spectrum Metal Sequestration

Md. Arifur Rahim,[†,§] Gan Lin,[†] Pietro Pacchin Tomanin,[†] Yi Ju,[†] Anders Barlow,[‡] Mattias Björnmalm,[†] and Frank Caruso[,†]*

[†]ARC Centre of Excellence in Convergent Bio-Nano Science and Technology, and the Department of Chemical Engineering, The University of Melbourne, Parkville, Victoria 3010, Australia

[‡]Materials Characterisation and Fabrication Platform, The University of Melbourne, Parkville, Victoria 3010, Australia

KEYWORDS: sequestration, sorbents, metal–phenolic gels, metal pollutants, catalysis

ABSTRACT

Metal contamination of water bodies from industrial effluents presents a global threat to the aquatic ecosystem. To address this challenge, metal sequestration via adsorption onto solid media has been explored extensively. However, existing sorbent systems typically involve energy-intensive syntheses and are applicable to a limited range of metals. Herein, a sorbent system derived from physically cross-linked polyphenolic networks using tannic acid and Zr^{IV} ions has been explored for high affinity, broad-spectrum metal sequestration. The network formation step (gelation) of the sorbent is complete within 3 min and requires no special apparatus. The key to this system design is the formation of a highly stable coordination network with an optimized metal–ligand ratio (1.2:1), affording access to a major portion of the chelating sites in tannic acid for capturing diverse metal ions. The sorbent system effectively sequesters 28 metals in single- and multi-element model wastes, with removal efficiencies exceeding 99% and is stable over a pH range of 1–9. Furthermore, it is demonstrated that this system can be processed as membrane coatings, thin films, or wet gels to capture metal ions, and that both the sorbent and captured metal ions can be regenerated or directly used as composite catalysts.

INTRODUCTION

Water pollution by heavy metals from various industrial effluents is a growing concern worldwide.[1,2] Human exposure to such environments can lead to a range of medical conditions including carcinogenesis, anemia, kidney damage, and cognitive impairment.[3–5] Additionally, the increasing consumption of precious metals, such as gold, palladium, or ruthenium, in industries, such as electronics and catalysis, is leading to resource depletion, thus emphasizing the

importance to reduce, reuse, and recycle these resources.[6,7] Therefore, there is current demand for the development of advanced technologies for the efficient removal and recycling of metals from industrial waste and contaminated water bodies.

Among the diverse processes in use for metal sequestration (such as chemical precipitation and ion exchange), adsorption is promising owing to its simplicity, ease of operation, and economic feasibility.[2] The ideal sorbent system for high-performance metal sequestration must meet a number of criteria. For instance, it needs to be inexpensive, non-hazardous, easily prepared and scalable, resistant to post-capture leaching, and stable in harsh conditions, and needs to exhibit high metal capture efficiency for a broad-spectrum metal ions.[8] However, fulfilling these criteria for a sorbent system remains challenging. Some recent materials have demonstrated excellent performance[9,10] but trade-offs between low cost, simple production and efficient broad-spectrum metal capture remain a key limitation for these materials. For example, metal–organic framework (MOF)-based sorbents demonstrate excellent metal capture performance but often require multi-day synthesis at high temperature and post-synthetic modification.[10]

In nature, plants respond to heavy metal toxicity via different mechanisms that include immobilization and chelation of the metal ions. Plants produce chelators, such as metallothioneins and phytochelatins,[11,12] that perform these tasks highly effectively. Inspired by this biological approach, herein, we present a sorbent system based on another class of plant-derived chelators, that is, polyphenols, for metal sequestration. This simple and high-performance sorbent system is based on our recently introduced metal–phenolic gels using tannic acid (TA) and Zr^{IV} ions.[13] These materials are prepared through coordination-driven assembly and leverage the versatile chemistry of TA (including reduction and chelation interactions)[14] to achieve a highly efficient metal–phenolic sorbent (MPS) system. The present MPS system

displays a combination of attributes: (i) it can sequester 28 metals both in single- and multi-element model wastes (a more diverse set than that of previously reported sorbents); (ii) its performance is on par or exceeds current high-performance systems (including capture efficiencies exceeding 99%, distribution coefficients (K_d) exceeding 4×10^5 mL g^{-1}, and maximum sorption capacities ranging from 400 to >1000 mg g^{-1} for key metals such as Au, Pb, and Hg); and (iii) it can be assembled quickly (<3 min), easily (no special apparatus needed), and inexpensively (using low-cost, off-the-shelf components). In addition to this set of attributes, the MPS system can be engineered into membrane coatings, thin films, or wet gels to further facilitate its application in diverse areas. Finally, the MPS system (and the captured metals) can be easily regenerated or directly used as composite catalysts for the decomposition of organic pollutants.

RESULTS AND DISCUSSION

Synthesis and Characterization. The fabrication of the MPS is based on a rapid sol–gel process that does not require intensive energy input or any special apparatus. Both constituents of the sorbent system are inexpensive, highly biocompatible, and abundant: TA is an ubiquitous plant polyphenol (Figure 1e)[14] and the concentration of Zr^{IV} in the earth's crust is ~0.02%, which is comparable to that of carbon.[15] The preparation of the MPS system is schematically presented in Figure 1a, b. After mixing the ligand (TA) and metal solutions, the TA/Zr^{IV} sol turned into a transparent gel within 3 min at 85 °C (at room temperature (25 °C), the gelation time was observed to be ~10 min). The MPS sorbent powders obtained (Figure 1f) from the dried TA/Zr^{IV} gels were subsequently examined for metal sequestration (Figure 1c, d). In contrast to our previous work on the gelation behavior of a TA/Zr^{IV} system at a molar ratio of 1:5,[13] the present MPS system was optimized with a TA/Zr^{IV} molar ratio of 1:1.2, which allowed a larger portion

(~80%) of the binding sites (i.e., catechol and gallol groups, Figure 1e) in TA to be available (i.e., non-crosslinked by Zr^{IV}) for the capture of incoming metals in the sorbent network (Figure 1d).

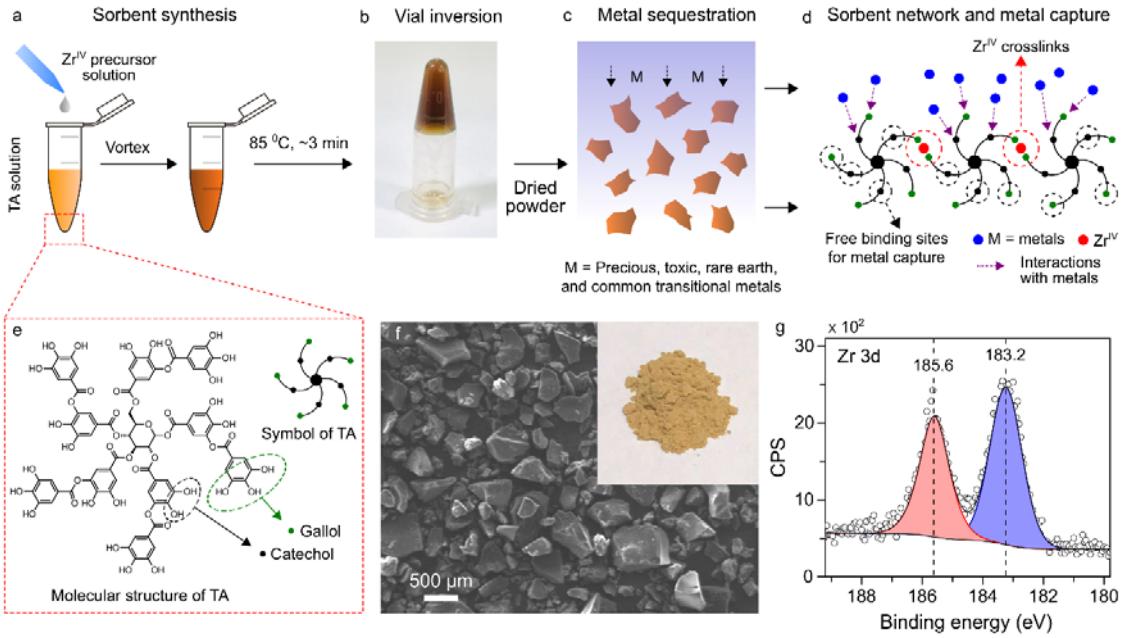

Figure 1. (a–c) Schematic illustration of the preparation of the MPS and subsequent application for metal sequestration. (d) Molecular view of the MPS network and metal sorption via interaction with free catechol and/or gallol groups of TA in the sorbent. (e) Molecular structure and schematic representation of TA. (f) Scanning electron microscopy image and photograph (inset) of the MPS powder. (g) Core-level X-ray photoelectron spectroscopy pattern of Zr^{IV} in the MPS.

The gelation of the MPS system was confirmed by the vial inversion test (Figure 1b) and rheological measurements (Figure S1). The in situ gelation (at room temperature, ~25 °C) was monitored by dynamic oscillatory rheology experiments—both the storage modulus (G') and loss modulus (G'') profiles displayed an increase with time and overlapped (Figure S1). The sol–gel transition occurred when $G' > G''$ after the G'/G'' crossover point. After the drying and washing

steps, the resulting MPS powder was subjected to further characterization. The Fourier transform infrared spectra of pure TA and the MPS (Figure S2) revealed notable differences. For example, the characteristic vibrational peaks of TA, that is phenolic C=O stretching at 1703.78 cm^{-1}, phenolic C–O stretching at 1533.40, 1444.63, 1310.05, and 1082.40 cm^{-1}, and phenolic O–H in-plane bending at 1179.76 cm^{-1} [16,17] were shifted to 1696.62, 1504.77, 1441.77, 1314.34, 1186.92, and 1060.92 cm^{-1}, respectively, in the MPS, indicating the coordination interactions involving Zr^{IV} and the catechol and/or gallol groups of TA in the sorbent network. The survey X-ray photoelectron spectroscopy (XPS) pattern revealed the presence of C 1s, O 1s, and Zr 3p and 3d peaks (Figure S3), which are consistent with the sorbent constituents. The Zr 3d peaks at binding energies (BEs) of 183.2 ($3d_{5/2}$) and 185.6 ($3d_{3/2}$) eV were detected in the core-level XPS pattern (Figure 1g) with a spin-orbit separation of 2.4 eV. Relative to the characteristic Zr 3d peaks for ZrO_2 at 182.3 ($3d_{5/2}$) and 184.7 ($3d_{3/2}$) eV,[18,19] the shift to the higher binding energies (~1.1 eV) in the MPS suggested the presence of catechol– and/or gallol–Zr^{IV} coordination bonding in the network; it is known that the BE of a central atom increases with increasing electronegativity of the attached atoms or groups.[20,21] Similar BE shifts for Zr-based coordination compounds, such as Zr^{IV}/phytic acid complexes, have been reported.[22] From the scanning electron microscopy image in Figure 1f, the particle size of the MPS ranged from 0.3 to 1.2 mm. The MPS system was stable in the pH range of 1–9, as evident from the flat spectral lines observed in the UV-visible absorption spectra (Figure S4), suggesting that there is no leaching of TA from the MPS (characteristic absorbance peaks of TA are found in the range of 220–400 nm[23]). Leaching of Zr^{IV} was also absent, as confirmed by inductively coupled plasma mass spectrometry (ICP-MS) analyses. The high stability of the TA/Zr^{IV} bulk network over the wide pH range (1–9) can be attributed to the strong catechol– and/or gallol–Zr^{IV} cross-links stemming from the high Lewis

acidity and oxidation state of Zr.[13,24] This is also consistent with the higher stability observed for Zr^{IV}/gallic acid MOFs when compared with the conventional Zr^{IV}/carboxylate MOFs.[14,24] High stability of a sorbent system, particularly in acidic conditions, is important: (i) as metal-contaminated wastewater is typically acidic in nature;[6,8] (ii) to prevent secondary pollution via leaching;[8] and (iii) as it offers the possibility to regenerate the sorbent via pH regulation.[10] (See also *Regeneration and Catalysis*)

Single- and Multi-Element Metal Capture Efficiency. To investigate the capture efficiency of the MPS system, the sorption experiments involved a library of metal ions that can be classified into four general categories: precious, toxic, rare earth, and common transition metals. The metal ion concentrations before and after sorption tests were determined using ICP-MS. As shown in Figure 2a–d, the MPS sequestered all 28 metal ions studied—precious metals (Au^{III}, Ag^{I}, Pd^{II}, In^{III}, Ru^{III}, and Os^{III}), toxic metals (Pb^{II}, Hg^{II}, and Cd^{II}), common transition metals (Ti^{III}, Ni^{II}, Fe^{III}, Cu^{II}, Zr^{IV}, Mn^{II}, Zn^{II}, and Ga^{III}), and rare earth metals (Ce^{IV}, Tb^{III}, Gd^{III}, Eu^{III}, La^{III}, Ho^{III}, Tm^{III}, Yb^{III}, Nd^{III}, Dy^{III}, and Er^{III})—in single-element model wastes, with removal efficiencies exceeding 99%. Note that the sorption experiments for all metal ions were performed at their pristine solution pH (4.8–5.8) except for Cu^{II}, Ni^{II}, and Zn^{II}. Initial sorption experiments with Cu^{II}, Ni^{II}, and Zn^{II} at their pristine pH (~4.5–4.8) resulted in removal efficiencies of 80–85%, which improved to >99% at pH 7. The higher removal efficiency is likely due to the higher deprotonated state of TA at the higher pH, which facilitate coordination interactions (see *Sorption Mechanism* for more details).[14,23] Thus, the results obtained at pH 7 for these three metals are reported in Figure 2c.

For metal sequestration, the affinity of a sorbent for a target metal ion can be expressed by K_d defined as follows:[25]

$$K_d = \frac{(C_i - C_f)}{C_f}\frac{V}{m}$$

where C_i and C_f are the initial and final equilibrium metal ion concentrations, respectively, V is the volume of the treated solution (mL), and m is the mass of the sorbent (g). Sorbent materials possessing K_d values of 1×10^4 mL g^{-1} are considered "very good" and values exceeding 1×10^5 mL g^{-1} are considered "excellent".[25,26] The K_d values determined for the MPS system for the 28 metal ions studied were within the range of 4×10^5 to 1×10^6 mL g^{-1}. To our knowledge, such values (above "excellent" in classification) for a diverse set of metals as reported herein have not been reported for other sorbent systems.

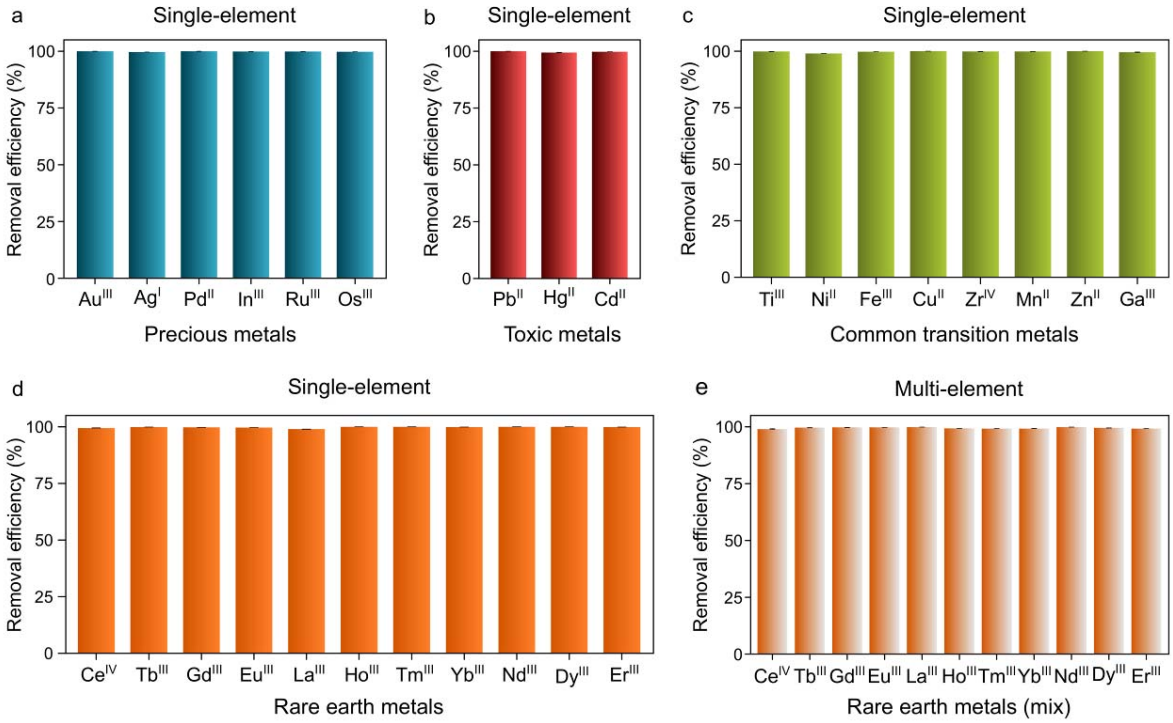

Figure 2. (a–d) Efficiency of the MPS system for the removal of different classes of metals from a single-element model waste. (e) Example of nonselective removal of rare earth metal ions from a multi-element rare earth metal mixture by the MPS. Conditions: Single–element study, MPS = 0.010 g; concentration of each metal ion = 10 ppm; volume = 10 mL; pH 7 for Cu^{II}, Ni^{II}, and

Zn^{II}, and pristine pH (4.8–5.8) for the remaining metal ions; multi–element study, MPS = 0.11 g; concentration of each metal ion = 10 ppm; volume = 10 mL; pristine pH of the mixture was ~5.1.

In addition to achieving high removal efficiency, it is important to consider the residual concentration of highly toxic metals in the treated water. According to the U.S. Environmental Protection Agency, the acceptable limit of Pb^{II} and Hg^{II} in drinking water is <2 ppb.[10,26,27] After treatment with the MPS, the concentrations of Pb^{II} and Hg^{II} in the model waste were reduced from 5 ppm (typical median concentration found in industrial effluents and wastewater)[10,28] to 0.4 (removal efficiency of ~99.998%) and 1.4 ppb (removal efficiency of ~99.97%), respectively, indicating the potential of the MPS system.

Similar removal efficiency levels (>99%) were also achieved in the multi-element sorption tests performed with the rare earth and precious metals (Figures 2e and S5), highlighting the broad-spectrum metal ion capturing ability of the MPS system, which can be attributed to the abundant catechol and gallol groups in the system that can form metal chelate/redox complexes (see *Sorption Mechanism* for more details).

Sorption Kinetics and Isotherm. Sorption kinetics and maximum sorption capacity are metrics that are also used to assess the performance of a sorbent. For convenience, Au^{III} and In^{III}, Pb^{II} and Hg^{II}, Tb^{III} and Gd^{III}, and Cu^{II} and Ni^{II} were selected as representatives of precious, toxic, rare earth, and common transition metals, respectively. Regardless of the metal category studied, the MPS showed fast sorption kinetics (Figures 3a–c, S6–S10), where the removal efficiency exceeded 90% within ~15 min and 99% after equilibrium at 2–4 h. The experimental data were fitted with the pseudo-second-order kinetic model[29] (see *Experimental Section*) with high correlation coefficients of >0.99 (Table S2). The fast sorption kinetics (for example, activated carbon typically requires 72 h to reach equilibrium)[30] of the MPS further suggests that the rate-

determining step for the sorption of metal ions onto the sorbent is mainly chemical in nature (see *Sorption Mechanism* for more details).

The sorption isotherms for the above representative metals were also measured and the experimental data were fitted with the Langmuir adsorption model[31] (Figures 3d–f, S11–S15, Table S2). The maximum sorption capacities (Figure 3g) determined from the sorption model for these metal ions were approximately 1350, 180, 424, 446, 404, 406, 135, and 149 mg g^{-1} for Au^{III}, In^{III}, Pb^{II}, Hg^{II}, Tb^{III}, Gd^{III}, Cu^{II}, and Ni^{II}, respectively. These values are higher than those achieved by many other sorbents and competitive to some of the highest-performing sorbents in the field (Table S3). Also note that, unlike the MPS, the high sorption capacities displayed by most sorbents in the literature are generally applicable to specific metal ions (rather than a range of metal ions).

Contaminated water bodies are typically multifarious in nature, that is, they contain multiple metal pollutants. Based on the applicability of the MPS to a wide range of metals (Figure 2e), the simultaneous removal efficiency of the MPS was studied for all four categories of metal ions. A mixture containing a total of 26 metal ions was used. Ag^{I} and Os^{III} were omitted because of the observed precipitation in the mixture (see *Experimental Section* for details). As shown in Figure 3h, the MPS system simultaneously captured 23 of the 26 metal ions studied with efficiencies above 99%. The removal efficiency for Ni^{II}, Cu^{II}, and Zn^{II} was slightly lower (~80%), as expected (and mentioned above), as the pristine pH of the mixture was ~5.

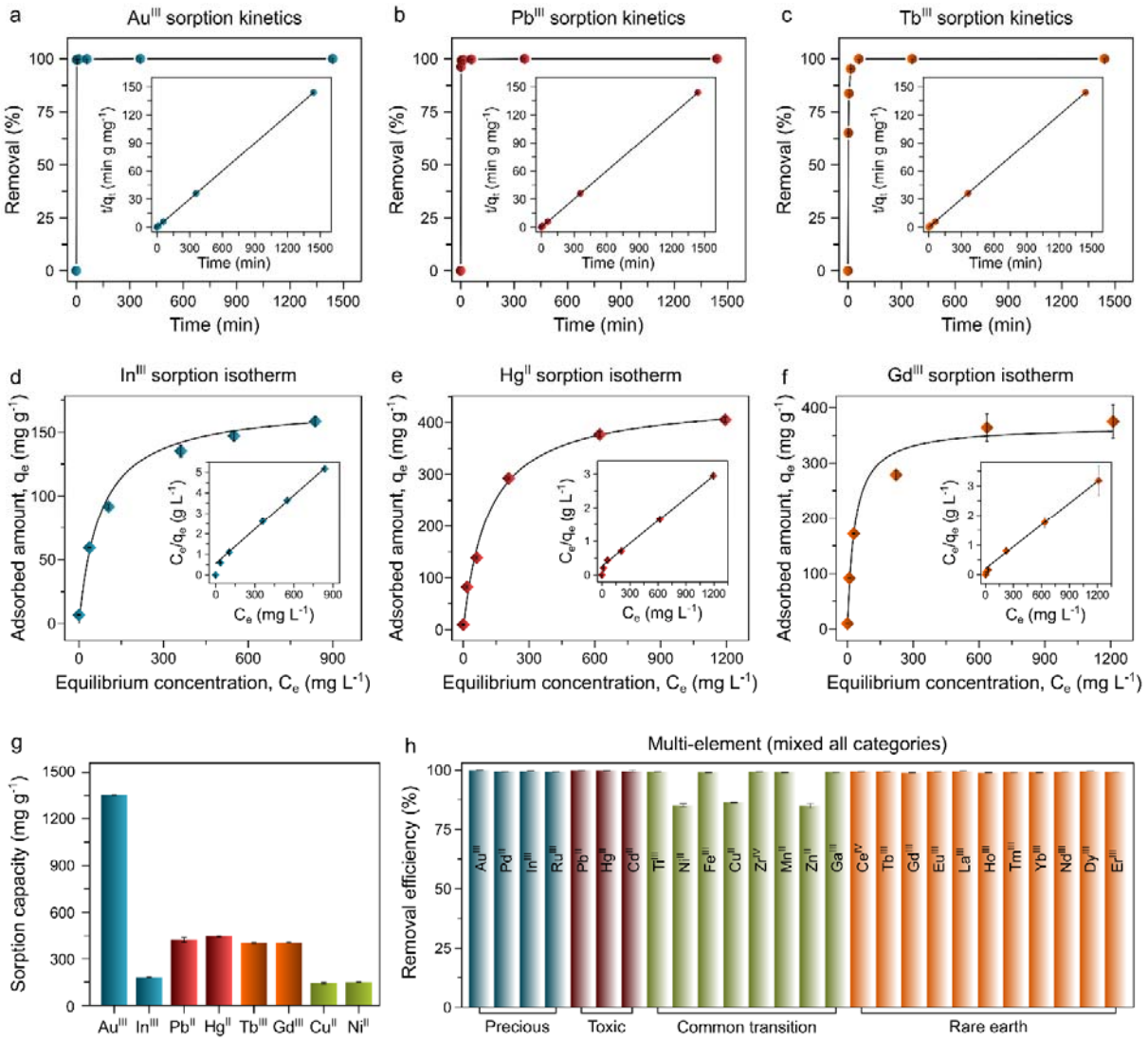

Figure 3. (a–c) (Au^{III}, Pb^{II}, and Tb^{III}) sorption kinetics of the MPS; insets show the linear pseudo-second-order kinetics fit of the data. (d–f) (In^{III}, Hg^{II}, and Gd^{III}) sorption isotherms of the MPS; insets show the linear fit of the Langmuir adsorption model. (g) Maximum sorption capacity calculated from the sorption model-fitted data for the representative metal ions. (h) Simultaneous removal of metals from multi-element model waste containing 26 metal ions by the MPS (conditions: MPS = 0.13 g; concentration of each metal ion in the mixture = 5 ppm; volume = 10 mL; pH ≈ 5).

Sorption Mechanism. XPS was used to probe the chemical interactions occurring during the sorption of various metal ions onto the MPS. The analyses provided two broad scenarios for the different metal categories studied. In the precious metal category, two distinct types of interactions were observed. The core-level Au 4f XPS spectra, as shown in Figure 4a (survey spectra are provided in Figure S16), revealed the BEs of Au $4f_{7/2}$ and Au $4f_{5/2}$ peaks at 84.3 and 88.1 eV, respectively, with a spin-orbit separation of 3.8 eV, that can be assigned to elemental Au^0.[32,33] Minor contributions from the ionic forms of Au^I (BE at 85.5 eV)[34] and Au^{III} (BE at 87.5)[34] were also observed, where the former is possibly caused by the incomplete reduction of some Au^{III} ions and the latter originates from the direct coordination with catechol and/or gallol binding sites. The redox interactions of TA with precious metals (e.g., Au^{III} and Ag^I) are well documented in the literature and are generally attributed to the redox potential matching of TA with these metals, leading to the reduction of the metal ions with the concomitant oxidation of gallol and/or catechol groups to quinones (Figure 4d).[35] In contrast, in the same category, In^{III} was captured within the MPS network via coordination to the catechol and/or gallol binding sites (Figures 4b and S16), as confirmed by the appearance of BE peaks at 445.7 ($3d_{5/2}$) and 453.3 ($3d_{3/2}$) eV (cf. In^0 at 443.8 ($3d_{5/2}$) and In^{III} in In_2O_3 at 444.7 ($3d_{5/2}$) eV).[36,37] Similarly, BE peaks of Hg 4f at 101.7 ($4f_{7/2}$) and 105.7 ($4f_{5/2}$) eV, with a spin-orbit separation of 4 eV, (Figure 4c) can be attributed to Hg^{II} species (as referenced to Hg^0 at 99.9 and Hg^{II} in HgO at 100.5 eV)[38,39] coordinated to catechol/gallol groups from TA in the MPS. For the other metal categories, coordination interactions were observed to be dominant (Figures S17–S27). For example, the BEs for Pb^{II}, and Tb^{III} and Gd^{III}, and Cu^{II} and Ni^{II} from the toxic, rare earth, and common transition metal categories, respectively, as detected from their XPS core-level spectra confirmed that their oxidation states could be assigned to their corresponding coordination complexes with

the catechol and/or gallol binding sites in the MPS (see relevant discussions in Figures S17–S27).

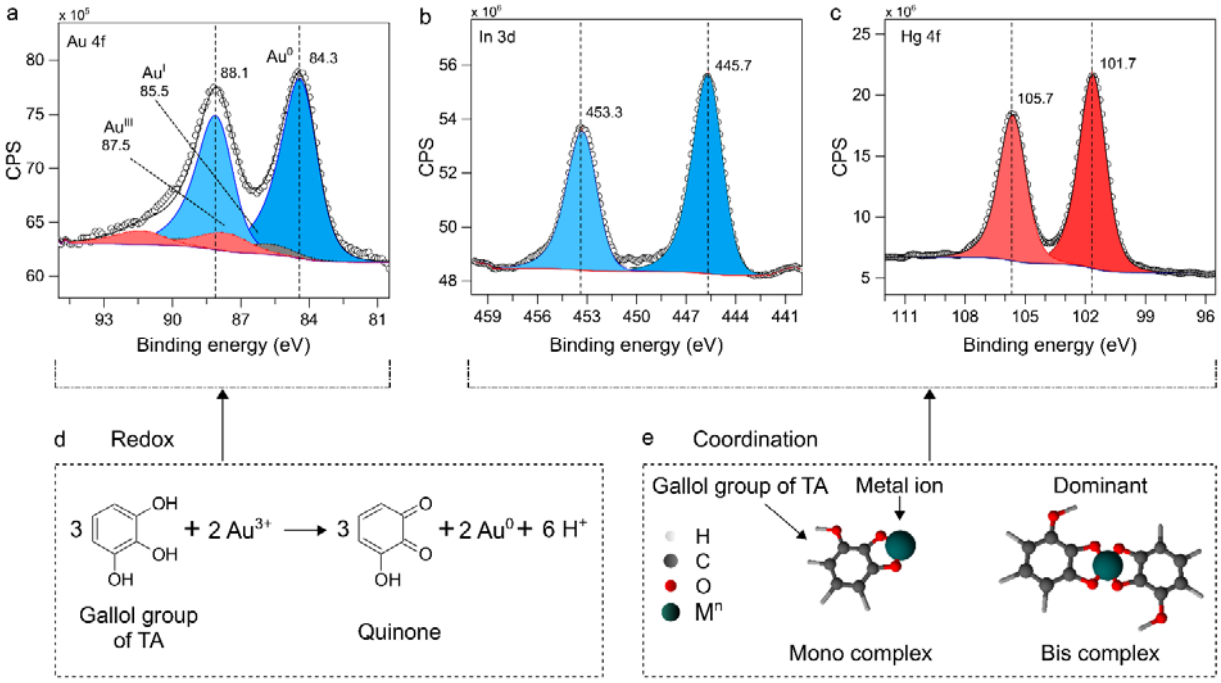

Figure 4. Core-level XPS spectra of Au 4f (a), In 3d (b), and Hg 4f (c). Proposed sorption mechanisms for the metals onto the MPS system: redox interactions (d) and coordination interactions (e).

Additionally, considering the TA/Zr molar composition (1:1.2) of the MPS system, the total amount of binding sites (catechol and /or gallol groups) available for metal capture in 1 g of the MPS is about 4 mmoles. For metals captured via coordination, if the mono-type coordination mode (i.e., each metal ion is attached to one catechol or gallol group, Figure 4e) dominates, the maximum sorption capacity values are expected to be approximately 459 (In^{II}), 829 (Pb^{II}), 802 (Hg^{II}), 636 (Tb^{III}), 629 (Gd^{III}), 254 (Cu^{II}), and 235 (Ni^{II}) mg g^{-1}. However, the maximum sorption capacities determined experimentally were roughly half of these values (Figure 3g, Table S3), suggesting that these metals were captured into the MPS via the bis-type coordination

mode (bis complex), wherein each metal ion is attached to two catechol or gallol groups, as shown in Figure 4e.

Processing Flexibility. Processing flexibility is another important aspect to consider in realizing the full potential of a sorbent system, as the metal sequestration medium may be required in different forms, such as thin films on solid surfaces or support membranes, depending on the application. Most of the current sorbent systems are intrinsically limited in this criterion and require additional materials (e.g., polymers) to process as thin films. Examples include MOFs, zeolites, and ion-exchange resins that are typically synthesized as solid particles[10,40,41] and as such are difficult to be processed as thin films without polymer excipients and additional processing steps. In contrast, the preparation of the present MPS system is based on a sol–gel route, possessing intrinsic solution processability, that enables the system to be processed as thin films on solid surfaces. Sorption experiments performed on the MPS-coated commercial filter membranes or glass substrates (film thickness of ~200 nm as measured by atomic force spectroscopy, Figure S28) with Ti^{III}, Fe^{III}, and Au^{III} as representative examples are shown in Figure 5. The color changes detected upon metal sorption were due to the characteristic ligand-to-metal charge transfer (LMCT) bands of Ti^{III}– and Fe^{III}–catechol/gallol complexes[13,42,43] and the surface plasmon resonance of Au^{0} nanoparticles.[35]

Furthermore, there has been recent interest in using supramolecular gels for environmental remediation owing to their highly solvated structure, which can provide high surface area and intimate contact with liquid phases containing pollutants and their rapid diffusion into the gel matrix.[2,3] Taking this into account, we demonstrate the use of the wet MPS gel (the pristine gel was subjected to a solvent exchange step with water) for metal ion removal. During the capture

of Fe^{III} ions into the gel matrix (Figure 5c), the gel turned blue–black owing to the characteristic LMCT band originating from the Fe^{III}–catechol/gallol complex formation.

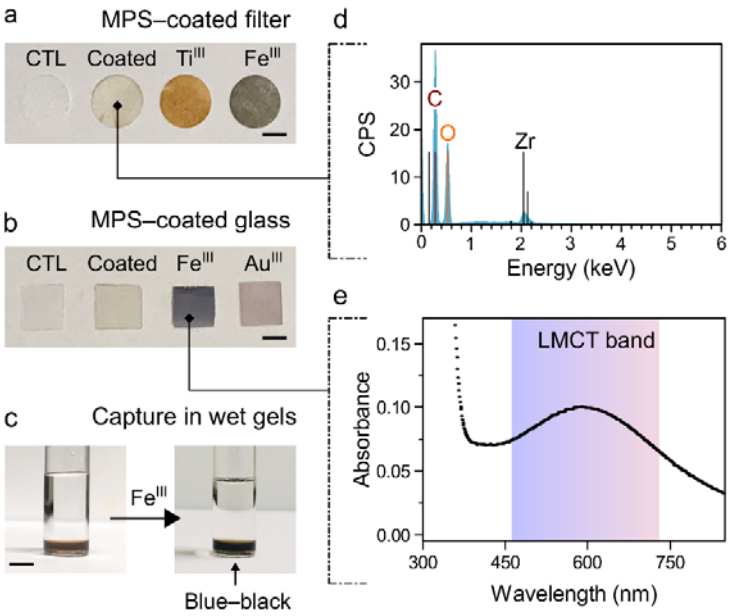

Figure 5. (a, b) Photographs illustrating the processing flexibility of the MPS system engineered into the MPS-coated commercial filter membranes or glass substrates and their subsequent use for metal sequestration. **(**c) Photograph showing the sequestration of Fe^{III} by the MPS gel. Scale bars are 5 mm. (d) Energy-dispersive X-ray spectroscopy pattern showing the presence of Zr^{IV} in the MPS-coated filter. (e) Characteristic absorbance spectrum after sorption of Fe^{III} onto the MPS-coated glass substrate. CTL, control.

Regeneration and Catalysis. Regeneration of sorbent materials is essential for durability and cyclic use. When the MPS sorption mechanism proceeds via coordination, the MPS sorbent system can be easily regenerated by washing in 0.1 M HCl. This leads to desorption of the adsorbed metal ions through destabilization of their coordination interactions with the MPS matrix, without perturbation of the TA–Zr^{IV} cross-links. However, for sorption occurring via redox interactions, a different desorption solution was necessary, that is, thiourea 1 M in 0.1 M

HCl solution.[44,45] The MPS sorbent could undergo a series of sorption–desorption cycles without loss in efficiency. For example, In^{III} and Tb^{III} (sorption via coordination) captured by the MPS were regenerated in four consecutive cycles (Figure 6a, b) without any detectable loss in efficiency when the sorption experiments were performed at a low metal concentration of 10 ppm. At a higher metal ion concentration (700 ppm; to reach the maximum sorption capacity of the MPS for each metal ion), the sorption capacity of the MPS could be retained, with minimal loss in efficiency (<2%), in four consecutive sorption–desorption cycles. However, for precious metals, such as Au^{III} captured via redox interactions, the MPS system showed a slightly lower regeneration efficiency—the removal efficiency of the MPS decreased from ~95 to ~88% after three consecutive sorption–desorption cycles (Figure S29). This reduced efficiency can be attributed to some irreversible structural changes in TA within the MPS via the formation of quinones and their intermediates during the redox interactions.

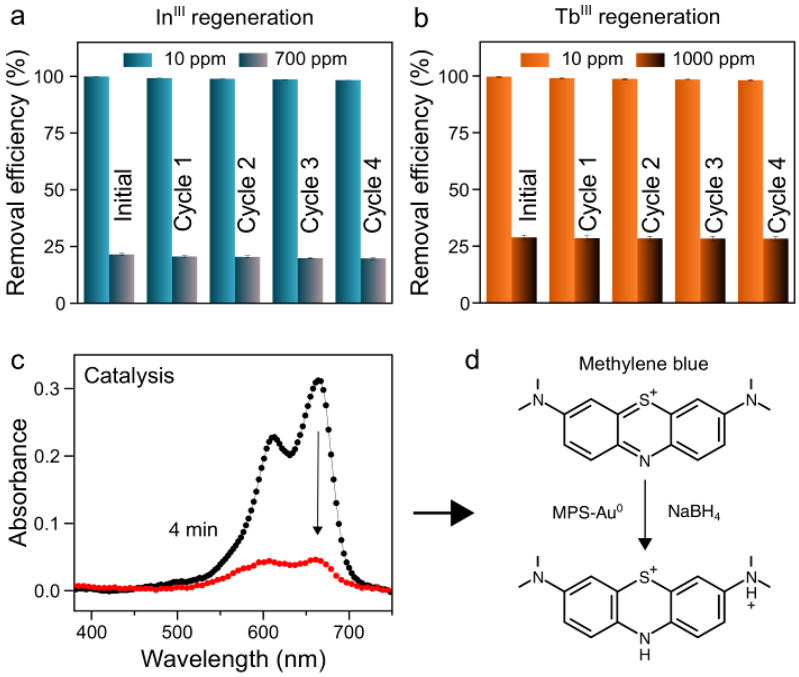

Figure 6. Regeneration of the MPS system, as investigated by the sorption–desorption cycles of In^{III} (a) and Tb^{III} (b) at different initial metal ion concentrations. UV–visible absorbance spectra (c) of the catalytic degradation of methylene blue in the presence of MPS–Au^0 (d).

We hypothesized that the capture of precious metals from water via redox-mediated formation of metallic species (as observed for some precious metals, for example Au^0 species after Au^{III} sorption in the MPS) could endow the sorbents with catalytic properties. Such properties may be useful for different and complementary applications including the decontamination of toxic organic pollutants. To test this hypothesis, the catalytic activity of the sorbents (MPS–Au^0 and MPS–Ag^0) toward the degradation of methylene blue (MB) and 4-nitrophenol (4-NP), respectively, was assessed after confirming the capture of precious metals and formation of the corresponding nanoparticles within the MPS network. MPS–Au^0 degraded MB (Figure 6c, d) and catalyzed the conversion of 4-NP into 4-aminophenol (4-AP) (Figure S30).

CONCLUSIONS

A robust sorbent system using tannic acid and Zr^{IV} with high sequestration performance was reported. The MPS sorbent system displayed distribution coefficients exceeding 4×10^5 mL g^{-1} with removal efficiencies of >99% for 28 metal ions studied. Considering the multifarious nature of polluted water streams, the simultaneous removal of 23 metals in multi-element model waste with high efficiency was also demonstrated. The sorbent system, of which the preparation is simple, rapid, and involves naturally abundant and inexpensive starting components, features high stability, high sorption capacity, fast sorption kinetics, and easy regeneration, making it potentially suitable for environmental remediation and precious metal recovery. Moreover, following the capture of precious metals, the resulting sorbent was demonstrated to perform as

composite catalysts for the degradation of organic pollutants. We are currently investigating the use of the MPS system for the sequestration of metalloid (such as arsenic) pollutants.

EXPERIMENTAL SECTION

Synthesis of the MPS. In a typical synthesis, aliquots of TA solution (300 μL, 60% w/v in ethanol, 600 mg mL^{-1}), tetrahydrofuran (THF) (120 μL), and Zr^{IV} precursor solution (180 μL, 0.735 M in 1:1 v/v of water/THF mixture) were mixed in a tube under vortex to achieve a TA/Zr^{IV} molar ratio of 1:1.2. The mixture was immediately placed in a preheated oven at 85 °C, and gelation occurred within 3 min as confirmed from the vial inversion test (at room temperature, 25 °C, the gelation time was ~10 min). The obtained gel samples were dried in a fume hood for 6 h and ground (~3 g sample) in a commercial micronizer (XRD-Mill McCrone, MEP Instruments) set at 50 W for 5 min. The ground powder samples were washed 3 times in water and freeze-dried to obtain the final sorbent samples.

Stability Tests for the MPS. MPS (0.005 g) samples were added to 1.5 mL tubes containing aqueous solutions (1 mL) of different pHs ranging from 1 to 9, and the tubes were kept on a rotating wheel (~40 rpm) for 24 h. The dispersions were filtered through 0.22 μm membrane filters and the filtrates were analyzed by UV-visible spectroscopy and ICP-MS to assess the leaching of TA and Zr^{IV} ions, respectively.

Metal Sorption from Single-Element Model Waste Systems. For the metal sorption experiments in single-element model waste systems, stock solutions of the metal ions were first prepared by dissolving the relevant metal salts (Table S1) in Milli-Q water. Then, in a typical sorption experiment, the MPS (0.010 g) was added into a 15 mL tube containing stock solution (10 mL) of the metal ion (10 ppm) and the tube was kept on a rotating wheel (~40 rpm) for 24 h. After the adsorption process, the mixture was filtered through a 0.22 μm membrane filter to

separate the MPS from the metal ion solution, and the filtrate was analyzed by ICP-MS to determine the metal concentration in the supernatant. The adsorption experiments were conducted at the intrinsic pH of the metal ion solution (10 ppm)—precious metals, 4.8–5.2; toxic metals, 5.5–5.8; rare earth metals, 5.2–5.5; and common transition metals, 4.5–5.1—except for the experiments involving Cu^{II}, Ni^{II}, and Zn^{II} that were conducted at pH 7. The removal efficiency for each metal ion studied was calculated using the following equation:

$$\text{Removal efficiency (\%)} = (C_i - C_f)/C_i \times 100$$

where C_i is the initial metal ion concentration and C_f is the final equilibrium metal ion concentration after adsorption onto the MPS.

Conducting sorption experiments with Cu^{II}, Ni^{II}, and Zn^{II} at their pristine pH (~4.5–4.8, 10 ppm) resulted in removal efficiencies of 80–85%, which improved to >99% at pH 7 (bis-tris buffer, 10 mM). Thus, only the results obtained from sorption experiments performed at pH 7 are reported.

Metal Sorption from Multi-Element Model Waste Systems. For the metal sorption experiments in multi-element model waste systems, stock solutions of the metal ions were prepared by dissolving the relevant metal salts (Table S1) in Milli-Q water. For each metal ion category studied, the metal stock solutions were mixed to obtain a final stock of 10 ppm for each metal ion. Then, for a given category, the MPS (0.11 g for rare earth and 0.04 g for precious metal categories) was added into a 15 mL tube containing stock solution (10 mL) of the mixed metal ions and the tube was kept on a rotating wheel (~40 rpm) for 24 h. Note that for the precious metal category, Os^{III} and Ag^{I} (due to the presence of metal chloride-based salts that lead to the formation of AgCl which is insoluble in water) were omitted because of the occurrence of precipitation in the mixture. Subsequently, the mixture was filtered through a 0.22 μm membrane

filter to separate the MPS from the metal ion solution, and the filtrate was analyzed by ICP-MS to determine the metal ion concentration.

Experiments involving all metal ion categories (a total of 26 metals, as Ag^{I} and Os^{III} were omitted as mentioned above) were also performed (MPS 0.13 g) as above with mixed metal ions at a concentration of 5 ppm for each.[10]

Sorption Kinetics Measurements. The MPS (0.010 g) was added into a 15 mL tube containing solution (10 mL) of the metal ion (10 ppm). The mixture was kept on a rotating wheel (~40 rpm) at room temperature (~25 °C) for 24 h. During the sorption period, aliquots of the suspension (300 μL) were filtered at specific time intervals through a 0.22 μm membrane filter, and the filtrates were analyzed by ICP-MS to determine the remaining metal content. The experimental data thus obtained were fitted with the pseudo-second-order kinetic model according to the following equation:[26]

$$t/q_t = 1/kq_e^2 + t/q_e$$

where q_t (mg g^{-1}) and q_e (mg g^{-1}) are sorption amounts of the metal ions at time t (min) and at equilibrium, respectively, and k (g mg^{-1} min^{-1}) is the rate constant for the pseudo-second-order equation.

Sorption Isotherm Tests. The MPS (0.010 g) was added into a 15 mL tube containing solution (10 mL) of the metal ion with varying concentrations from 10 to 2000 ppm. The mixture was kept on a rotating wheel (~40 rpm) at room temperature (~25 °C) for 24 h. Subsequently, the mixture was filtered through a 0.22 μm membrane filter to separate the MPS from the metal ion solution, and the filtrate was analyzed by ICP-MS to determine the remaining metal concentration. The experimental data were fitted with the Langmuir isotherm model described by the following equation:[10]

$$c_e/q_e = 1/K_L q_m + c_e/q_m$$

where q_e (mg g^{-1}) is the amount of metal ions adsorbed onto the sorbent at equilibrium, c_e (mg L^{-1}) is the metal ion concentration at equilibrium, q_m (mg g^{-1}) is the maximum sorption capacity at monolayer coverage, and K_L is the Langmuir constant.

Preparation of the MPS Films. To obtain the MPS films coated on a glass substrate, aliquots of TA solution (300 μL, 60% w/v in ethanol, 600 mg mL^{-1}), THF (120 μL), and Zr^{IV} precursor solution (180 μL, 0.735 M in 1:1 v/v water/THF mixture) were mixed in a tube under vortex for 15 s to achieve a TA/Zr^{IV} molar ratio of 1:1.2. The mixture was immediately diluted (2 fold) under vortex by ethanol and an aliquot of this mixture (50 μL) was spread onto a standard microscope glass slide using a cell scrapper and allowed to dry. For the MPS membrane preparation, cellulose filter papers were dipped into the above mixture for 2 min and allowed to dry.

Before the sorption experiments, the MPS-coated membranes or glass substrates were washed twice in Milli-Q water. Sorption experiments were performed using 50 ppm of the desired metal salt solutions (10 mL, pH 3.5–4.5) and dipping the substrates into the metal solutions for 6 h.

Regeneration of the MPS. The MPS (0.010 g) was added into a 15 mL tube containing solution (10 mL) of the metal ion (In^{III}, Tb^{III}, or Au^{III}). The mixture was kept on a rotating wheel (~40 rpm) at room temperature (~25 °C) for 24 h. Subsequently, the mixture was filtered through a 0.22 μm membrane filter to separate the MPS from metal ion solutions, and the filtrate was analyzed by ICP-MS to determine the remaining metal concentration. The In^{III}- and Tb^{III}-captured MPS samples were then treated with 0.1 M HCl (5 mL) for 6 h (desorption step) and washed 3 times with water before the next sorption step. This process was repeated for 4 cycles (sorption–desorption) for the metal ion studied. For the sorption steps, two sets of experiments

with different concentrations for In^{III} (10 and 700 ppm) and Tb^{III} (10 and 1000 ppm) were performed. For Au^{III}, the concentration used for Au^{III} was 1000 ppm, and after each desorption step (thiourea 1 M in 0.1 M HCl solution, 5 mL), the MPS samples were treated with 1 mM of $NaBH_4$ (5 mL, for 5 min) to reduce the quinones back to gallol and catechol groups. The sorption–desorption cycle was repeated 3 times.

Catalysis Experiments. The Au^{III}- and Ag^{I}-captured MPS samples (MPS–Au^0 and MPS–Ag^0, respectively) obtained from the sorption experiments with 10 ppm metal concentrations (0.01 g MPS) were washed with water for several times, and their catalytic activity toward the degradation/reduction of MB was evaluated.

An MB solution (2 mL, 100 μM) containing freshly prepared $NaBH_4$ (20 μM) (reducing agent), was added to the washed pellets of MPS–Au^0 and the absorbance of the MB solution at ~665 nm was measured over time. The MB solution turned colorless within 5 min. A 4-NP solution (2 mL, 0.4 mM) containing freshly prepared $NaBH_4$ (40 mM) (reducing agent), was added to the washed pellets of MPS–Ag^0 and the absorbance of 4-NP solution at ~400 nm was measured over time. Along with the decrease in the peak intensity at ~400 nm, a peak at ~300 nm appeared over time, suggesting the formation of 4-AP. For the control experiments, which were conducted in the absence of the MPS-based samples, no change in absorbance (that correlates to the catalytic activity) was observed.

ASSOCIATED CONTENT

Materials and characterization; additional characterization data for the MPS sorbents, including rheology, XPS, FTIR, and UV–vis absorbance; additional data regarding removal efficiency, sorption kinetics, sorption isotherm, and sorption mechanisms (XPS) for different metals; and

AFM film thickness and catalysis experimental data. The Supporting Information is available free of charge.

The authors declare no competing financial interest.

AUTHOR INFORMATION

Corresponding Author

*E-mail: fcaruso@unimelb.edu.au

Present Addresses

[§]Present address: School of Chemical Engineering, University of New South Wales (UNSW), Sydney Campus, NSW 2052, Australia

ACKNOWLEDGMENT

This research was conducted and funded by the Australian Research Council (ARC) Centre of Excellence in Convergent Bio-Nano Science and Technology (project number CE140100036) and an ARC Discovery Project (DP170103331). F.C. acknowledges the award of a National Health and Medical Research Council Senior Principal Research Fellowship (GNT1135806). This work was performed in part at the Materials Characterisation and Fabrication Platform (MCFP) at The University of Melbourne and the Victorian Node of the Australian National Fabrication Facility. The authors acknowledge the use of facilities within the Monash X-ray Platform and Dr. Andrew Mitchell (MCFP, The University of Melbourne) for the helpful discussions regarding the inductively coupled plasma mass spectrometry studies.

References

1. Bilal, M.; Shah, J. A.; Ashfaq, T.; Gardazi, S. M. H.; Tahir, A. A.; Pervez, A.; Haroon, H.; Mahmood, Q. Waste Biomass Adsorbents for Copper Removal from Industrial Wastewater – A Review. *J. Hazard. Mater.* **2013**, *263*, 322–333.
2. Okesola, B. O.; Smith, D. K. Applying Low-Molecular Weight Supramolecular Gelators in an Environmental Setting – Self-Assembled Gels as Smart Materials for Pollutant Removal. *Chem. Soc. Rev.* **2016**, *45*, 4226–4251.
3. Alizadehgiashi, M.; Khuu, N.; Khabibullin, A.; Henry, A.; Tebbe, M.; Suzuki, T.; Kumacheva, E. Nanocolloidal Hydrogel for Heavy Metal Scavenging. *ACS Nano* **2018**, *12*, 8160–8168.
4. Lee, J.-C.; Son, Y.-O.; Pratheeshkumar, P.; Shi, X. Oxidative Stress and Metal Carcinogenesis. *Free Radical Biol. Med.* **2012**, *53*, 742–757.
5. Liu, J.; Du, X. Fast Removal of Aqueous Hg(II) with Quaternary Ammonium-Functionalized Magnetic Mesoporous Silica and Silica Regeneration. *J. Mater. Chem.* **2011**, *21*, 6981–6987.
6. Das, N. Recovery of Precious Metals through Biosorption — A Review. *Hydrometallurgy* **2010**, *103*, 180–189.
7. Dodson, J. R.; Parker, H. L.; Muñoz García, A.; Hicken, A.; Asemave, K.; Farmer, T. J.; He, H.; Clark, J. H.; Hunt, A. J. Bio-Derived Materials as a Green Route for Precious & Critical Metal Recovery and Re-Use. *Green Chem.* **2015**, *17*, 1951–1965.
8. Bacelo, H. A. M.; Santos, S. C. R.; Botelho, C. M. S. Tannin-Based Biosorbents for Environmental Applications – A Review. *Chem. Eng. J.* **2016**, *303*, 575–587.
9. Bolisetty, S.; Mezzenga, R. Amyloid–Carbon Hybrid Membranes for Universal Water Purification. *Nat. Nanotechnol.* **2016**, *11*, 365–371.
10. Peng, Y.; Huang, H.; Zhang, Y.; Kang, C.; Chen, S.; Song, L.; Liu, D.; Zhong, C. A Versatile MOF-Based Trap for Heavy Metal Ion Capture and Dispersion. *Nat. Commun.* **2018**, *9*, 187.
11. Rauser, W. E. Structure and Function of Metal Chelators Produced by Plants. *Cell Biochem. Biophys.* **1999**, *31*, 19–48.
12. Cobbett, C. S. Phytochelatins and Their Roles in Heavy Metal Detoxification. *Plant Physiol.* **2000**, *123*, 825.
13. Rahim, M. A.; Björnmalm, M.; Suma, T.; Faria, M.; Ju, Y.; Kempe, K.; Müllner, M.; Ejima, H.; Stickland, A. D.; Caruso, F. Metal–Phenolic Supramolecular Gelation. *Angew. Chem. Int. Ed.* **2016**, *55*, 13803–13807.
14. Rahim, M. A.; Kristufek, S. L.; Pan, S.; Richardson, J. J.; Caruso, F. Phenolic Building Blocks for the Assembly of Functional Materials. *Angew. Chem. Int. Ed.* **2019**, *58*, 1904–1927.
15. Blumenthal, W. B. Zirconium Chemistry in Industry. *J. Chem. Educ.* **1962**, *39*, 604.
16. Çakar, S.; Özacar, M. Fe–Tannic Acid Complex Dye as Photo Sensitizer for Different Morphological ZnO Based DSSCs. *Spectrochim. Acta, Part A* **2016**, *163*, 79–88.
17. Ranoszek-Soliwoda, K.; Tomaszewska, E.; Socha, E.; Krzyczmonik, P.; Ignaczak, A.; Orlowski, P.; Krzyzowska, M.; Celichowski, G.; Grobelny, J. The Role of Tannic Acid and Sodium Citrate in the Synthesis of Silver Nanoparticles. *J. Nanopart. Res.* **2017**, *19*, 273.
18. Dementjev, A. P.; Ivanova, O. P.; Vasilyev, L. A.; Naumkin, A. V.; Nemirovsky, D. M.; Shalaev, D. Y. Altered Layer as Sensitive Initial Chemical State Indicator. *J. Vac. Sci. Technol., A* **1994**, *12*, 423–427.
19. Sleigh, C.; Pijpers, A. P.; Jaspers, A.; Coussens, B.; Meier, R. J. On the Determination of Atomic Charge via ESCA Including Application to Organometallics. *J. Electron. Spectrosc. Relat. Phenom.* **1996**, *77*, 41–57.
20. Escamilla, R.; Huerta, L. X-Ray Photoelectron Spectroscopy Studies of Non-Stoichiometric Superconducting NbB_{2+x}. *Supercond. Sci. Technol.* **2006**, *19*, 623–628.
21. Egelhoff, W. F. Core-Level Binding-Energy Shifts at Surfaces and in Solids. *Surf. Sci. Rep.* **1987**, *6*, 253–415.
22. Song, J.; Zhou, B.; Zhou, H.; Wu, L.; Meng, Q.; Liu, Z.; Han, B. Porous Zirconium–Phytic Acid Hybrid: A Highly Efficient Catalyst for Meerwein–Ponndorf–Verley Reductions. *Angew. Chem. Int. Ed.* **2015**, *54*, 9399–9403.

23. Rahim, M. A.; Ejima, H.; Cho, K. L.; Kempe, K.; Müllner, M.; Best, J. P.; Caruso, F. Coordination-Driven Multistep Assembly of Metal–Polyphenol Films and Capsules. *Chem. Mater.* **2014**, *26*, 1645–1653.
24. Mouchaham, G.; Cooper, L.; Guillou, N.; Martineau, C.; Elkaïm, E.; Bourrelly, S.; Llewellyn, P. L.; Allain, C.; Clavier, G.; Serre, C.; Devic, T. A Robust Infinite Zirconium Phenolate Building Unit to Enhance the Chemical Stability of Zr MOFs. *Angew. Chem. Int. Ed.* **2015**, *127*, 13495–13499.
25. Shin, Y.; Fryxell, G. E.; Um, W.; Parker, K.; Mattigod, S. V.; Skaggs, R. Sulfur-Functionalized Mesoporous Carbon. *Adv. Funct. Mater.* **2007**, *17*, 2897–2901.
26. Li, B.; Zhang, Y.; Ma, D.; Shi, Z.; Ma, S. Mercury Nano-Trap for Effective and Efficient Removal of Mercury(II) from Aqueous Solution. *Nat. Commun.* **2014**, *5*, 5537.
27. Zhang, Q.; Yang, Q.; Phanlavong, P.; Li, Y.; Wang, Z.; Jiao, T.; Peng, Q. Highly Efficient Lead(II) Sequestration Using Size-Controllable Polydopamine Microspheres with Superior Application Capability and Rapid Capture. *ACS Sustainable Chem. Eng.* **2017**, *5*, 4161–4170.
28. Mondal, M. Removal of Pb(II) from Industrial Wastewater by Using Various Natural Materials – A Review. *Int. J. Sustainable. Dev. Plann.* **2008**, *3*, 377–393.
29. Ho, Y. S.; McKay, G. Pseudo-Second Order Model for Sorption Processes. *Process Biochem.* **1999**, *34*, 451–465.
30. Sánchez-Polo, M.; Rivera-Utrilla, J. Adsorbent–Adsorbate Interactions in the Adsorption of Cd(II) and Hg(II) on Ozonized Activated Carbons. *Environ. Sci. Technol.* **2002**, *36*, 3850–3854.
31. Foo, K. Y.; Hameed, B. H. Insights into the Modeling of Adsorption Isotherm Systems. *Chem. Eng. J.* **2010**, *156*, 2–10.
32. Brown, M. A.; Fujimori, Y.; Ringleb, F.; Shao, X.; Stavale, F.; Nilius, N.; Sterrer, M.; Freund, H.-J. Oxidation of Au by Surface OH: Nucleation and Electronic Structure of Gold on Hydroxylated MgO(001). *J. Am. Chem. Soc.* **2011**, *133*, 10668–10676.
33. Turner, N. H.; Single, A. M. Determination of Peak Positions and Areas from Wide-Scan XPS Spectra. *Surf. Interface Anal.* **1990**, *15*, 215–222.
34. Sylvestre, J. P.; Poulin, S.; Kabashin, A. V.; Sacher, E.; Meunier, M.; Luong, J. H. T. Surface Chemistry of Gold Nanoparticles Produced by Laser Ablation in Aqueous Media. *J. Phys. Chem. B* **2004**, *108*, 16864–16869.
35. Ahmad, T. Reviewing the Tannic Acid Mediated Synthesis of Metal Nanoparticles *J. Nanotechnol.* **2014**, *2014*, 1–11.
36. Faur, M.; Faur, M.; Jayne, D. T.; Goradia, M.; Goradia, C. XPS Investigation of Anodic Oxides Grown on p-Type InP. *Surf. Interface Anal.* **1990**, *15*, 641–650.
37. Kim, Y. J.; Jin, S. B.; Kim, S. I.; Choi, Y. S.; Choi, I. S.; Han, J. G. Effect of Oxygen Flow Rate on ITO Thin Films Deposited by Facing Targets Sputtering. *Thin Solid Films* **2010**, *518*, 6241–6244.
38. Hutson, N. D.; Attwood, B. C.; Scheckel, K. G. XAS and XPS Characterization of Mercury Binding on Brominated Activated Carbon. *Environ. Sci. Technol.* **2007**, *41*, 1747–1752.
39. Hua, X.-y.; Zhou, J.-s.; Li, Q.; Luo, Z.-y.; Cen, K.-f., Gas-Phase Elemental Mercury Removal by CeO_2 Impregnated Activated Coke. *Energy Fuels* **2010**, *24*, 5426–5431.
40. Yee, K.-K.; Reimer, N.; Liu, J.; Cheng, S.-Y.; Yiu, S.-M.; Weber, J.; Stock, N.; Xu, Z. Effective Mercury Sorption by Thiol-Laced Metal–Organic Frameworks: in Strong Acid and the Vapor Phase. *J. Am. Chem. Soc.* **2013**, *135*, 7795–7798.
41. Szostak, R. *Molecular Sieves*. Springer: New York, 1989.
42. Rahim, M. A.; Björnmalm, M.; Bertleff-Zieschang, N.; Besford, Q.; Mettu, S.; Suma, T.; Faria, M.; Caruso, F. Rust-Mediated Continuous Assembly of Metal–Phenolic Networks. *Adv. Mater.* **2017**, *29*, 1606717.
43. Rahim, M. A.; Kempe, K.; Müllner, M.; Ejima, H.; Ju, Y.; van Koeverden, M. P.; Suma, T.; Braunger, J. A.; Leeming, M. G.; Abrahams, B. F.; Caruso, F. Surface-Confined Amorphous Films from Metal-Coordinated Simple Phenolic Ligands. *Chem. Mater.* **2015**, *27*, 5825–5832.

44. Groenewald, T. The Dissolution Of Gold in Acidic Solutions of Thiourea. *Hydrometallurgy* **1976**, *1*, 277–290.
45. Nakajima, A.; Sakaguchi, T. Uptake and Recovery of Gold by Immobilized Persimmon Tannin. *J. Chem. Technol. Biotechnol.* **1993**, *57*, 321–326.

Table of Content Graphic

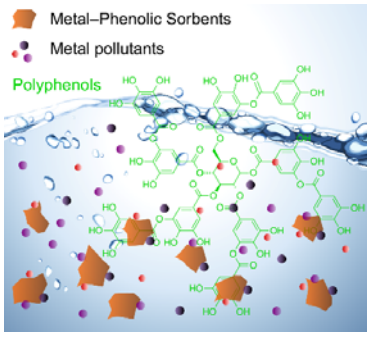

Author/s:
Rahim, MA; Lin, G; Tomanin, PP; Ju, Y; Barlow, A; Bjornmalm, M; Caruso, F

Title:
Self-Assembly of a Metal-Phenolic Sorbent for Broad-Spectrum Metal Sequestration

Date:
2020-01-08

Citation:
Rahim, M. A., Lin, G., Tomanin, P. P., Ju, Y., Barlow, A., Bjornmalm, M. & Caruso, F. (2020). Self-Assembly of a Metal-Phenolic Sorbent for Broad-Spectrum Metal Sequestration. ACS APPLIED MATERIALS & INTERFACES, 12 (3), pp.3746-3754. https://doi.org/10.1021/acsami.9b19097.